Mechanical Properties of Ultrananocrystalline Diamond Thin Films Relevant to MEMS/NEMS Devices

by H.D. Espinosa, B.C. Prorok, B. Peng, K.H. Kim, N. Moldovan, O. Auciello, J.A. Carlisle, D.M. Gruen and D.C. Mancini

ABSTRACT—The mechanical properties of ultrananocrystalline diamond (UNCD) thin films were measured using microcantilever deflection and membrane deflection techniques. Bending tests on several free-standing UNCD cantilevers, 0.5 μm thick, 20 μm wide and 80 μm long, yielded elastic modulus values of 916–959 GPa. The tests showed good reproducibility by repeated testing on the same cantilever and by testing several cantilevers of different lengths. The largest source of error in the method was accurate measurement of film thickness. Elastic modulus measurements performed with the novel membrane deflection experiment (MDE), developed by Espinosa and co-workers, gave results similar to those from the microcantilever-based tests. Tests were performed on UNCD specimens grown by both micro and nano wafer-seeding techniques. The elastic modulus was measured to be between 930–970 GPa for the microseeding and between 945–963 GPa for the nanoseeding technique. The MDE test also provided the fracture strength, which for UNCD was found to vary from 0.89 to 2.42 GPa for the microseeded samples and from 3.95 to 5.03 for the nanoseeded samples. The narrowing of the elastic modulus variation and major increase in fracture strength is believed to result from a reduction in surface roughness, less stress concentration, when employing the nanoseeding technique. Although both methods yielded reliable values of elastic modulus, the MDE was found to be more versatile since it yielded additional information about the structure and material properties, such as strength and initial stress state.

KEY WORDS—Thin films, nanomaterials, experimental techniques, fracture, size effects

Introduction

Silicon has been the dominant material in the microelectronics revolution of the 20th century and has been the precursor to the microelectromechanical/ nanoelectromechanical systems (MEMS/NEMS) revolution currently underway. It has been the material of choice for current MEMS devices, mainly because devices can be fashioned using standard microfabrication techniques.[1,2] However, Si is not the best choice for devices where friction and wear are present since its poor mechanical and tribological properties limit its performance.[3,4] Thus, new and robust materials with exceptional and tailorable properties must be sought to meet the stringent demands that MEMS/NEMS devices require.

Diamond Films for Micro and Nano Devices

Carbon in its various forms, specifically diamond, may become a key material for the manufacturing of MEMS/NEMS devices in the 21st century. The new ultrananocrystalline diamond (UNCD) developed at Argonne National Laboratory[5] is emerging as one of the most promising forms of diamond with unique multifunctional properties. The UNCD films are grown using a microwave plasma chemical vapor deposition (CVD) technique involving a new CH_4/Ar chemistry. The process yields films with extremely small grain size (3–5 nm), significantly smaller than nanocrystalline diamond films (30–100 nm grain size) produced by the conventional CH_4/H chemistry.[6,7] The films possess many of the outstanding physical properties of diamond, i.e., they exhibit exceptional hardness, extremely low friction coefficient and wear, high thermal and electrical conductivity (the latter when deposited with nitrogen[8]), high electrical resistance when grown with hydrogen addition to the CH_4/Ar plasma, and high chemical inertness, optical transmittance, electrical carrier mobility, and dielectric breakdown strength.

UNCD is characterized by a unique microstructure of sp^3-bonded grains and atomic grain boundaries (2–4 Å) with substantial sp^2 coordination. Preliminary results have shown that this unique microstructure results in outstanding mechanical properties (~97 GPa hardness and 967 GPa Young's modulus, which are similar to single-crystal diamond[9]), unique tribological properties (coefficient of friction of the order of ~0.02–0.03[10]), and field-induced electron emission (threshold voltage ~2–3 V μm^{-1} [11]). In addition, n-type doping of UNCD thin films, a long sought goal of researchers in diamond thin-film research, has been demonstrated, further broadening the range of applications of UNCD by achieving significant electrical conduction via nitrogen doping.[8,12] UNCD also exhibits unique inert electrochemical and biocompatible properties that make it suitable for biological applications.[13]

Preliminary work by investigators at Argonne National Laboratory has demonstrated the feasibility of fabricating

H.D. Espinosa (espinosa@northwestern.edu) (SEM Member) is a Professor, B.C. Prorok (SEM Member) is an Assistant Professor, B. Peng is a PhD Candidate, and K.H. Kim is a PhD Candidate, Department of Mechanical Engineering, Northwestern University, Evanston, IL 60208-3111. N. Moldovan is a Research Professor, O. Auciello is a Senior Scientist, J.A. Carlisle is a Senior Scientist, D.M. Gruen is a Senior Scientist, and D.C. Mancini is a Senior Scientist, Materials Science and Experimental Facilities Divisions, Argonne National Laboratory, Argonne, IL 60439.

Original manuscript submitted: December 19, 2002.
Final manuscript received: December 19, 2002.

two-dimensional (2D) and three-dimensional (3D) MEMS components that can be the basis for the fabrication of complete MEMS/NEMS devices.[11,14,15] Components, such as cantilevers, and multilevel devices, such as microturbines, have already been produced. These preliminary developments are promising steps toward full-scale application of UNCD components in functional MEMS devices. However, before full-scale integration can occur, several intrinsic material properties, such as elastic modulus, plasticity and fracture of undoped and doped UNCD, must be well characterized to fully exploit the potential of this material.

Microscale Mechanical Testing

Several mechanical testing schemes exist for examining the microscale mechanical properties of materials and structures. Extensive reviews exist on the subject.[16–18] Bending tests on micromachined beams were first performed by Weihs et al.[19] and repeated by others.[20,21] The method involves deflecting a cantilever-like beam fixed at one end to the substrate. A nanoindenter is used to deflect the beam and measures the load–deflection response. From this information, the stiffness of the beam is found and can be used to determine the elastic modulus of the material. Special attention should be placed on accurately measuring the beam dimensions as well as designing dimensions and testing conditions to minimize boundary, Poisson, and stress concentration effects.

The membrane deflection experiment (MDE), developed by Espinosa et al.,[22–24] is a novel microscale mechanical test for evaluating elasticity, plasticity, and fracture of thin films. It works by stretching a free-standing thin-film membrane in a fixed–fixed configuration where the membrane is attached at both ends and spans a micromachined window beneath; see Fig. 1(a). A nanoindenter applies a line-load at the center of the span to achieve deflection. Simultaneously, deflection is recorded by the nanoindenter displacement sensor and by an interferometer focused on the bottom side of the membrane through-view window in the wafer; see Fig. 1(b). The geometry of the membranes is such that it contains tapered regions to eliminate boundary failure effects. The basic architecture can be described as double-dog-bone. The result is direct tension, in the absence of strain gradients, of the gaged region. From this measurement, we determine mechanical properties such as Young's modulus, residual stress state, and yield and fracture stresses.

In this paper, we use microcantilever deflection and the membrane deflection experiment techniques to gain a better understanding of the elastic modulus and strength of UNCD thin films. We have taken special care to design different specimen characteristics for each technique in an attempt to minimize effects in each that may hinder accurate property measurements.

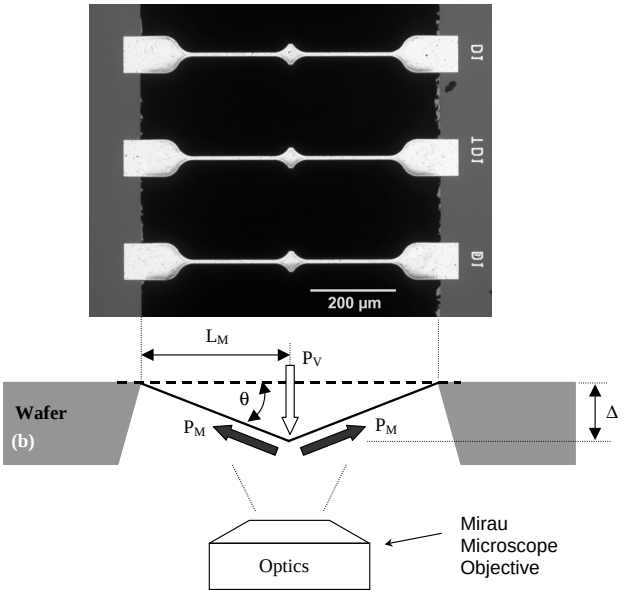

Fig. 1—(a) Optical image of three as-microfabricated MDE membranes; (b) side view of the MDE test showing vertical load being applied by the nanoindenter, PV, the membrane in-plane load, PM, and the position of the Mirau microscope objective

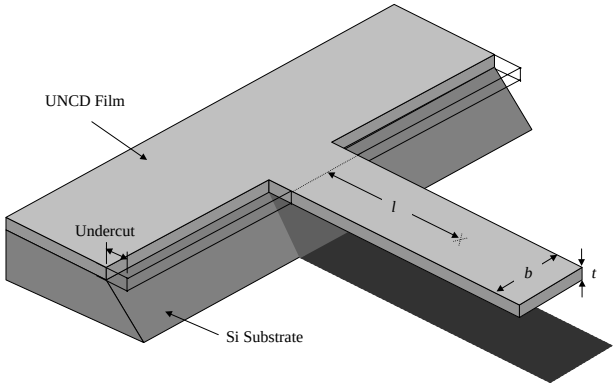

Fig. 2—Schematic 3D view of a free-standing cantilever structure. Geometric parameters are defined in the text.

Experimental Procedure

Specimen Design

Two types of specimens were used in this study. The first is a free-standing, thin-film cantilever structure made of UNCD with film thickness ranging from 0.55 to 0.65 μm. The film is grown directly onto a Si substrate as described below. Figure 2 shows a 3D schematic view of the cantilever structure. The dimensions of the cantilever are defined on the figure with *t* as the thickness, *b* as the width (20 μm for all cantilevers), and *l* as the cantilever length at the point of contact during deflection. The overall length of the cantilevers is 200 μm. The structure of the cantilevers contained an etching undercut that resulted in the specimens having a "T" shape (Fig. 2). This is accounted for in the data reduction procedure and is described later. The second type of specimen consists of specially designed double-dog-bone, free-standing membranes as shown in Fig. 1(a). Specimens with a width of ~13.5 μm were tested.

UNCD Film Growth and Specimen Microfabrication

The UNCD films were produced by a microwave plasma-assisted CVD technique developed at Argonne National Laboratory. Details of the synthesis are given in Gruen.[5] The

procedure yields UNCD films with grains 3–5 nm in diameter. UNCD films 0.5–0.6 μm thick were made to fabricate the cantilevers and the MDE specimens.

The cantilevers and MDE specimens were microfabricated using standard procedures. The following is a summary of the steps used in fabricating the UNCD cantilevers. A similar procedure was used to fabricate the MDE specimens.

1. Seeding the Si wafer and UNCD growth (0.5–0.6 μm).
2. Deposition of 300 nm Al by sputtering. Al is used as mask material due to its resistance to oxygen RIE.
3. Photoresist spin-coating with S 1805; exposure with Karl Suss MA6; developing; postbaking.
4. Wet chemical etching of Al.
5. O_2reactive ion etching (RIE), 50 mTorr, 200 W, until the exposed UNCD is etched away. During the etching, the photoresist is also removed. Removal of Al mask using wet etching.
6. Si wafer KOH etching from the front side (90 min, KOH 30% at 80°C) using the UNCD pattern as a masking layer. Cantilevers were so released. Underetching of UNCD cantilevers is possible due to a slight misalignment of the Si wafer <110> direction with respect to the cantilever structure.

Characterization Protocol

Both cantilever and membrane specimen structures were characterized by a variety of techniques. Dimensions of the cantilevers were measured with a translation stage possessing a resolution of 1 μm or better. The thickness of both structures was measured with a discrete wavelength ellipsometer and verified by cross-section scanning electron microscopy (SEM). Characterization of the out-of-plane initial cantilever shape was carried out by scanning the surface with a MicroXAM 3-D surface profilometer. Scans were also made after testing to identify permanent changes in cantilever deflection. Both were performed at identical temperature and humidity conditions. Evaluation of surface roughness was necessary to ascertain its effect on determining the cross-sectional area and to ascertain the effect of seeding on the resulting thin-film surface characteristics. Therefore, root-mean-square (rms) values of the film surface roughness were measured via atomic force microscopy (AFM).

Due to intrinsic strains and differences in thermal expansion coefficient between the UNCD film and the Si substrate, $\alpha_{UNCD} = 1.5 \times 10^{-6}\ ^{\circ}K^{-1}$ and $\alpha_{Si} = 2.5 \times 10^{-6}\ ^{\circ}K^{-1}$, the membranes exhibited an upward, out-of-plane buckling, shown in Fig. 3(a). The out-of-plane shape was characterized by interferometry. Figure 3(b) shows a typical profile exhibited by the membranes. This information is valuable in determining the height and point of contact between the indenter tip and membrane as well as the deflection where the straining of the membrane begins, described later in the Data Reduction section.

A final feature in the characterization of the UNCD film is non-uniformities that exist in the specimens due to the wafer seeding process required for UNCD deposition. Two seeding processes were used in the experiments described in this paper. One such process involved mechanical polishing of the Si substrate surface with micrometer-size diamond powder. This seeding process resulted in diamond particles generating defect sites on the substrate surface that, in turn, initiated film growth and at the same time led to scratch-like marks on the surface of the UNCD film; see the optical microscope image of a UNCD film in Fig. 3(a). These scratches produce stress concentrations detrimental to the film strength. A second seeding process consisted of the ultrasonic deposition of nanosized diamond powder on the Si substrate. This process significantly reduced the film roughness and eliminated scratch-like features on the surface of the film. We will discuss quantitative measurements in the Results section.

Mechanical Testing

Mechanical testing involved deflection of thin-film UNCD cantilevers and stretching of thin-film UNCD membranes with a nanoindenter. The cantilever deflection was carried out at different characteristic cantilever lengths and the MDE test was performed on specimens with different widths. Details of the MDE testing procedure were reported in Espinosa et al.[22–24] In both techniques, a nanoindenter deflected the specimens to a prescribed value. Load and deflection are recorded by the nanoindenter in both cases. For the MDE tests, deflection is also recorded by an interferometer. Although the two match well, the interferometer allows the experiment to be viewed *in situ* and important time signatures such as point of tip–membrane contact and membrane failure are determined.

Data Reduction

The raw data obtained from the tests were processed to obtain the quantities of interest. For instance, in both cantilever and membrane deflection tests the load obtained from the nanoindenter was properly reduced to remove thermal drift and support spring stiffness of the nanoindenter column. This procedure is described elsewhere.[22–26] The resulting load–deflection curve was then analyzed using cantilever and membrane formulae. In the case of the cantilever tests, the initial linear part of the curve was used to measure stiffness. Using this value and the standard stiffness equation for deflection of a uniform beam, with plate modulus to account for the large width to length ratio, the Young's modulus of the film was identified, namely

$$k = \frac{Eb}{4(1-\nu^2)}\left(\frac{t}{l}\right)^3, \tag{1}$$

where k is the stiffness, E is the Young's modulus, b is the cantilever width, ν is the Poisson's ratio, t is the thickness and l is the length of the cantilever at the point of contact. However, since the Poisson's ratio for diamond is 0.07, the Poisson effect can be ignored and the equation becomes that of a uniform beam.

In order to account for the T-shaped geometry of the cantilevers, finite element analyses (FEA) were performed using ANSYS 5.7 to obtain beam stiffness. The structure was meshed with SHELL63 elements. A Young's modulus of 1000 GPa and a Poisson's ratio of 0.07 were used as input parameters accounting for material properties. The simulated concentrated load was applied at the free-end and deflection at this point was used for the calculation of the T-shaped beam stiffness.

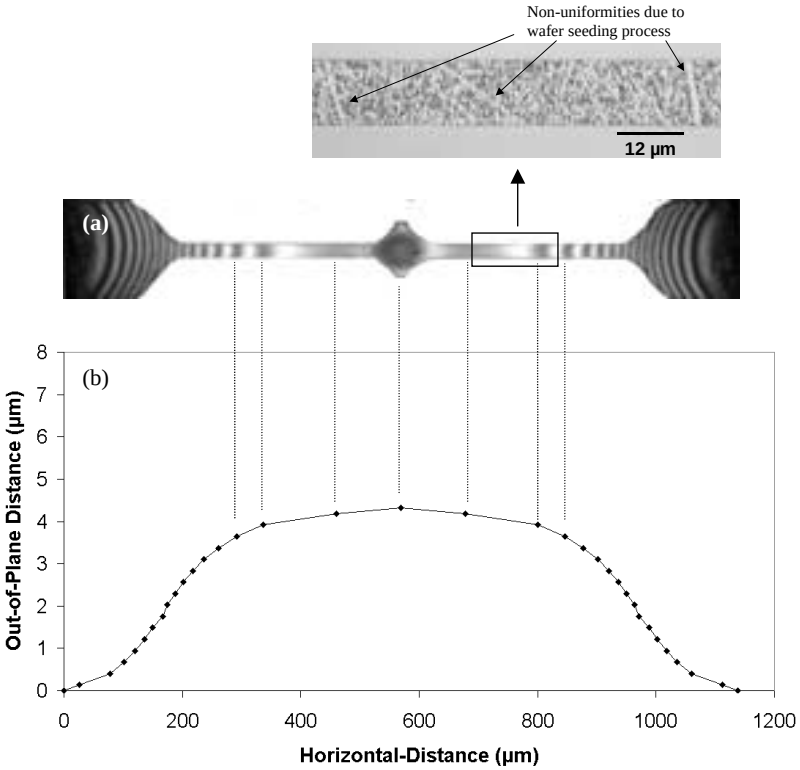

Fig. 3—(a) Typical optical interferometric image showing the out-of-plane bulging of the UNCD membranes; (b) *x-z* profile generated from a λ/2 (270 nm) height difference between fringes. The expansion of the gaged region in (a) shows scratch-like marks resulting from the wafer-seeding process.

By equating the numerically computed T-shaped beam stiffness to that of an equivalent beam with uniform width, b, and equivalent length, l_{eq}, given by

$$l_{eq} = l + \alpha l_u, \tag{2}$$

the parameter α was computed. In the above equation, l is the true cantilever length, and l_u is the length of the undercut (see Fig. 2). As the length of undercut varies depending on the local conditions of microfabrication, the equivalent length also changes. The coefficient α was then calculated for a series of undercut lengths (see Table 1) so that an equivalent length can be easily obtained for a particular measured undercut length.

The data reduction of the MDE results was identical to that described in Espinosa et al.[25] A brief summary is given here. The procedure involves applying a line-load, with a nanoindenter, at the center of the spanning membrane. Simultaneously, an interferometer focused on the bottom side of the membrane records the deflection. The result is direct tension in the gaged regions of the membrane with load and deflection being measured independently. The load in the plane of the membrane is found as a component of the vertical nanoindenter load by the following equations

$$\tan\theta = \frac{\Delta}{L_M} \tag{3}$$

and

$$P_M = \frac{P_V}{2\sin\theta}, \tag{4}$$

where, from Fig. 1(b), θ is the angle of rotation, Δ is the displacement of the membrane upon application of the load, L_M is the membrane half-length, P_M is the load in the plane of the membrane, and P_V is the load measured by the nanoindenter. Once P_M is obtained, the Cauchy stress, $\sigma(t)$, can be computed from

$$\sigma(t) = \frac{P_M}{A}, \tag{5}$$

where A is the cross-sectional area of the membrane in the gage region.

The interferometer yields vertical displacement information in the form of monochromatic images taken at periodic intervals (see Fig. 4). The relationship for the distance between interference fringes, δ, is related through the wavelength, λ, of the monochromatic light used. By finding the average distance between the number of fringes that are in the focal plane of the interferometer, an overall strain, $\varepsilon(t)$, for the membrane can be computed from the following relation:

$$\varepsilon(t) = \frac{\sqrt{\delta^2 + (\lambda/2)^2}}{\delta} - 1. \tag{6}$$

The initial shape of the UNCD specimens was that of a buckled membrane bowed upward, i.e., out of the wafer plane. This will be described in greater detail in the Results and Discussion section. Due to this shape, additional parameters were needed in the data reduction. This came in the form of identifying the height above the plane of the wafer, where the tip makes contact with the membrane (state 1 in Fig. 5), as

TABLE 1—VALUES OF COEFFICIENT α FOR DIFFERENT UNDERCUT LENGTHS

Undercut l_u (μm)	α	Undercut l_u (μm)	α
1	0.9419720	11	0.6224173
2	0.9100470	12	0.6017031
3	0.8711258	13	0.5826886
4	0.8318138	14	0.5651856
5	0.7942204	15	0.5490268
6	0.7590671	16	0.5340668
7	0.7266350	17	0.5201758
8	0.6969248	18	0.5072441
9	0.6697979	19	0.4951707
10	0.6450402	20	0.4838710

E = 1000 GPa and ν = 007 were used in the calculations.

well as the complete length of the membrane in its out-of-plane configuration. These parameters are used to determine the deflection required before uniform axial stretching of the membrane begins (state 3 in Fig. 5). This part of the procedure consists of using interferometry to determine the membrane profile and height above the wafer plane (see Fig. 3). The second step is to calculate the half-length of the membrane based upon its out-of-plane shape. This information is needed in order to compute the deflection required for stretching of the membrane to start (Δ_s), state 3 in Fig. 5. This state identifies the starting point of the computed stress–strain curve. The deflection Δ_s is computed by equating the measured upward membrane half-length (state 1 in Fig. 5) and the downward deformed shape (state 3 in Fig. 5). Note that a small but finite downward load is required to bring the specimen from state 1 to state 3. This implies that the buckled membrane has an initial non-uniform stress distribution, through the thickness, that must be overcome before a true membrane state develops.

Results and Discussion

The validity of the load calibration of the nanoindenter was confirmed via a microcantilever deflection test on a single-crystal (110) Si cantilever, for which the elastic properties are well characterized; i.e., $E_{[111]}$ = 185 GPa, $E_{[110]}$ = 170 GPa and $E_{[100]}$ = 130 GPa.[27] The structure used was a commercially available AFM tapping-mode tip (Digital Instrument, Co.). Figure 6 shows optical images of the top and bottom views of the tip architecture. As with the UNCD cantilevers, the AFM tip is configured in a "T" shape. Dimensions of the tip are shown in Fig. 6 where b = 46.62 μm, b_2 = 197.93 μm, t = 4.1 μm, l = 100 μm, l_u = 12μm, and the taper around the top edge is 5.0 μm in width and 100 nm deep. Numerical simulations were performed with these dimensions and the equivalent length, l_{eq}, was found to be 82.58 μm. Figure 7 shows the load–deflection curve for a cantilever test length of 80 μm. The stiffness, k, from different tests was found to be between 2.58×10^{-4} to 2.61×10^{-4} mN nm^{-1}.

The dimensions of the AFM cantilever are such that it can be approximated either as a plate or as a beam. Thus, the elastic modulus was calculated with and without considering the Poisson effect. Using eq (1) and a Poisson's ratio of 0.27 the elastic modulus was then calculated to be between 166–168 GPa. Without considering the Poisson effect, the modulus was found to be 179–181 GPa. These values are in close agreement to that of the [110] direction for Si, i.e., 170 GPa, which is along the length of the cantilever. Even though plate theory yielded values slightly closer to that of the literature modulus, the AFM cantilever geometry is between both cases. These results provide confidence on the ability and sensitivity of the nanoindenter to probe microscale specimens whose stiffness is on the order of or below the nanoindenter column stiffness of about 100 N m^{-1}.

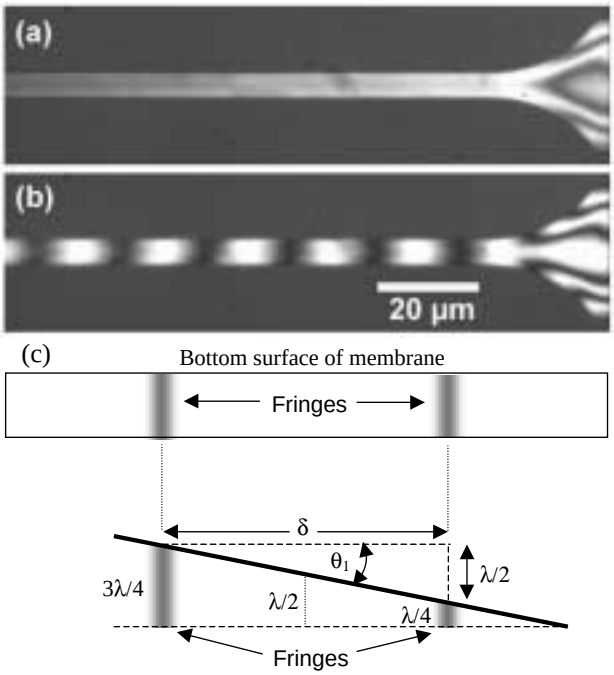

Fig. 4—Monochromatic images of the bottom side of the membranes showing an unloaded membrane (a) and a membrane under load which has developed fringes (b). (c) is a schematic representation showing the relationship between distance between fringes (δ) and vertical displacement.

Specimen Characterization

Figure 8(a) shows a SEM image of the fabricated UNCD cantilevers. From this view, the trench etched into the Si substrate to release the cantilevers is visible. Discernible is a slight undercutting of the diamond film, which is highlighted by white lines in Fig. 8(a) and schematically shown in the cross-section represented in Fig. 8(b). This is likely due to a

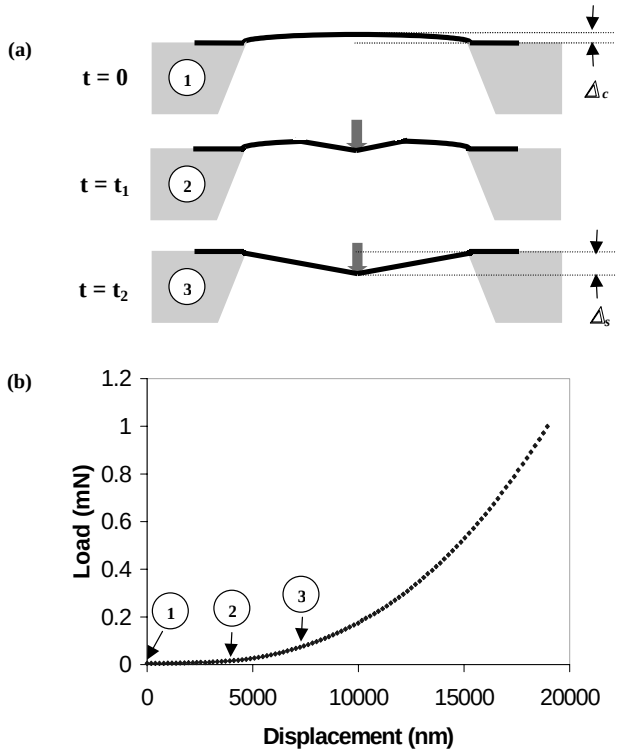

Fig. 5—(a) Schematic representations of the side view of the MDE test at three different states. The first state corresponds to the buckled membrane with deflection Δ_c at the middle of the span. The second state is associated to a downward deflection equal and opposite to the buckled deflection Δ_c. State 3 corresponds to a downward membrane deformation, with deflection Δ_s, in which the membrane length is equal to the membrane length in the buckled configuration (state 1). These three states are shown on the load-displacement curve in (b).

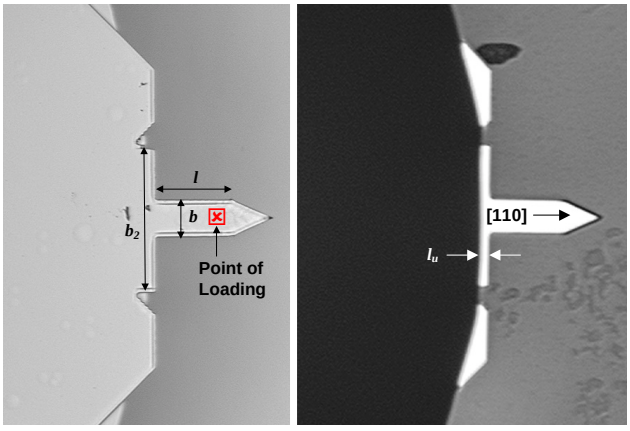

Fig. 6—Optical images of (a) the top view and (b) the bottom view of a silicon AFM tapping-mode tip. Undercut length is labeled as l_u.

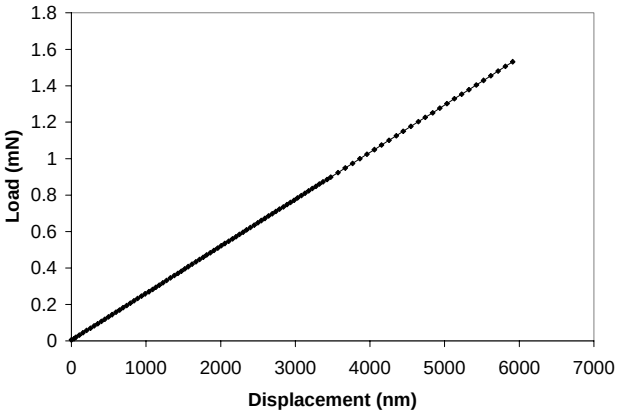

Fig. 7—Load-displacement curve for single-crystal silicon cantilever used to verify the nanoindenter load calibration

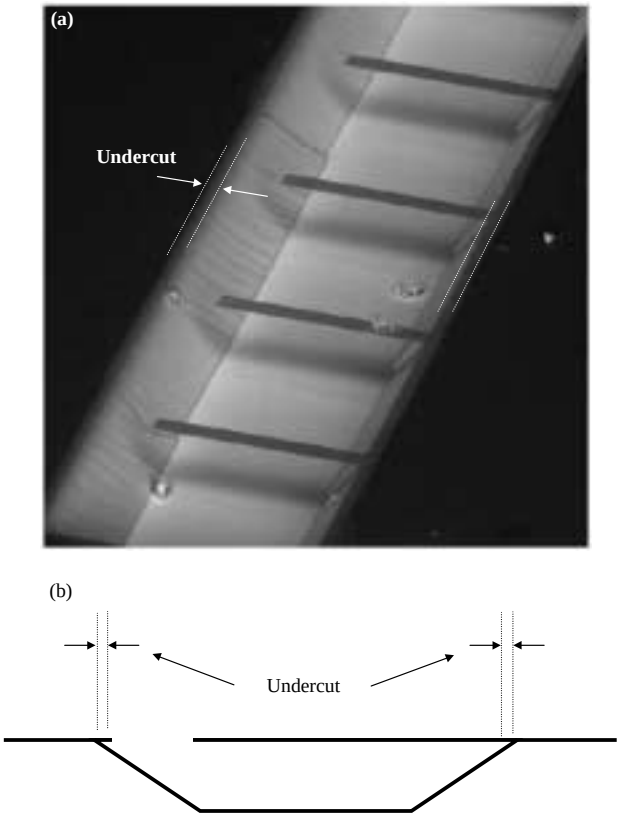

Fig. 8—(a) SEM image of the free-standing cantilevers; (b) schematic side view illustrating the undercut of the UNCD film

slight misalignment of the (110) wafer direction with respect to the cantilever structure defined by the photolithographic mask. The effect of this undercut requires that a calculation of an effective length be made for the cantilevers as discussed in the Data Reduction section. The undercut varied from die to die, in the range of 11–15 μm. Undercut values for individual cantilevers are given in Table 1. Figure 9(a) shows a head-on view of the end of a UNCD cantilever and Fig. 9(b) shows a close-up of the as-etched surface. All tested cantilevers had a length of 200 μm and a width of 20 μm.

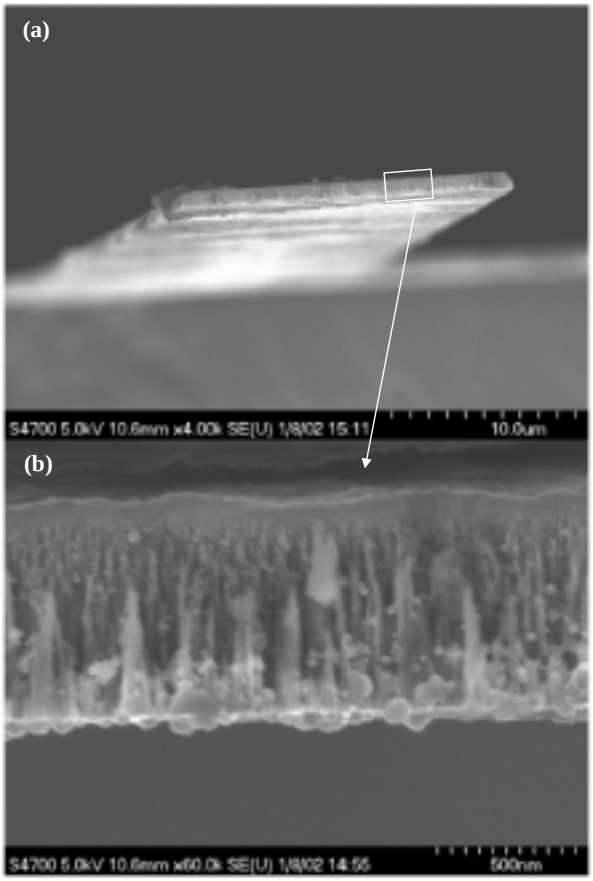

Fig. 9—SEM image of the free end (a), and zoom to show thickness and quality of the etched surfaces (b)

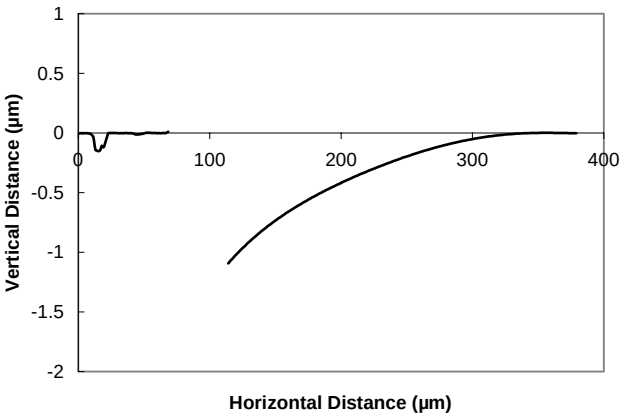

Fig. 10—Vertical profile of a typical UNCD cantilever. Note that the vertical axis is scaled differently than the horizontal axis to adequately display the initial cantilever shape.

One of the most important dimensions of the cantilevers in relation to the experiments discussed here is their thickness. We can see that when eq (1) is expressed in terms of the elastic modulus, the film thickness becomes cubed in the denominator. Small errors in this value, which is in the submicrometer regime for the tested UNCD films, can then create larger errors in modulus. To this end, each cantilever thickness was individually and carefully measured by discrete wavelength ellipsometry. Values for different cantilevers range from 0.57 to 0.64 μm and are listed in Table 2.

Another relevant parameter is the curvature of the as-released UNCD cantilevers. Figure 10 shows a typical as-released UNCD cantilever deflection as a function of the horizontal distance along the cantilever. This curve represents the vertical cross-section along the cantilever length. All cantilevers exhibited a downward deflection of varying magnitude. The exact cause of the curvature after release is not known, but it is believed to result from residual stresses arising during deposition and corresponding thermal expansion mismatch when cooled to room temperature. Profiles of cantilever initial shape were made and compared to post-test cantilever profiles.

The surface roughness of UNCD films used for both the microcantilever deflection and the MDE tests were evaluated using AFM. A determination of the rms surface roughness was necessary to gage its effect on measured properties. Figures 11(a) and (b) are 3D plots of the UNCD surface profile for typical, as-deposited, UNCD for microseeding and nanoseeding, respectively. Figures 11(c) and (d) show cross-sectional analysis used to measure the surface roughness of each. Five different sections were taken yielding a rms surface roughness value of approximately 80 nm for microseeded UNCD and 18 nm for the nanoseeded UNCD.

An important aspect of the UNCD MDE specimens was that each membrane bowed upward, i.e., out of the wafer plane. As mentioned earlier, this is believed to result from the difference in thermal expansion coefficients, between the film and Si wafer, such that cooling down from the deposition temperature, approximately 800°C, resulted in the Si shrinking more than the UNCD film. The film curvature is indicative of a gradient of residual stresses across the film thickness. Figure 3(a) shows a typical interferometric image and Fig. 3(b) the as-generated x-z profile. This profile was obtained from the knowledge that the vertical distance between two dark fringes is half of the wavelength of the monochromatic green light used in the imaging ($\lambda/2$ = 270 nm). From this profile the height above the plane of the wafer, Δ_c, was determined. Also, the profile was used to measure the actual length of the curved membrane, which is used to determine the downward deflection, Δ_s, corresponding to the beginning of uniform specimen straining. Figure 12 shows a series of optical images taken at different time intervals during a typical UNCD membrane deflection experiment. A schematic side view of the membrane is shown to the right of each frame. The first frame shows the state of the membrane just before contact is made. The successive frames show contact and deflection of the membrane. The process occurs in a smooth manner as seen by the inflection point, denoted by the arrows, moving toward the fixed end of the membrane. The final frame shows the deflection where uniform stretching of the membrane begins. As mentioned earlier, this state can be determined by computing the deflection Δ_s. This state represents the point from which the film stress–strain response was computed.

Cantilever Deflection Experiments

Figure 13 shows the load–deflection response of a typical cantilever loaded at a length of 80 μm. The plot begins with a sudden increase in load to 2 μN, which is believed to result from attractive forces and vapor condensation as the nanoindenter tip approaches the cantilever surface. Load

TABLE 2—VALUES OF INDIVIDUAL CANTILEVER DIMENSIONS, MEASURED, STIFFNESS, AND CALCULATED ELASTIC MODULUS

	ID	t (μm)	l (μm)	l_u (μm)	l_{eq} (μm)	k (N/m)	E (GPa)
(a)	80-A1	0.6305	80.0	15.32	88.2	1.70	936
	80-A2	0.5655	80.0	12.41	87.2	1.25	916
	80-A3	0.5800	80.0	11.42	86.9	1.43	959
	80-A4	0.5910	80.0	10.00	86.4	1.52	956
	80-A5	0.6420	80.0	15.01	88.2	1.80	938
	80-A6	0.6270	80.0	14.12	87.9	1.68	928
	80-A7	0.6110	80.0	11.61	87.1	1.59	924
(b)	60-B	0.6420	60.0	15.01	68.2	3.93	937
	80-B	0.6420	80.0	15.01	88.2	1.80	938
	100-B	0.6420	100.0	15.01	108.2	1.01	957
	120-B	0.6420	120.0	15.01	128.2	0.61	958
(c)	80-C.1	0.5910	80.0	10.00	86.4	1.52	956
	80-C.2	0.5910	80.0	10.00	86.4	1.49	931
	80-C.3	0.5910	80.0	10.00	86.4	1.51	943
	80-C.4	0.5910	80.0	10.00	86.4	1.50	937

Subset (a) are individual cantilevers with l = 80 μm, (b) are tests on the same cantilever with different length l, and (c) are tests on the same cantilever with identical length l.

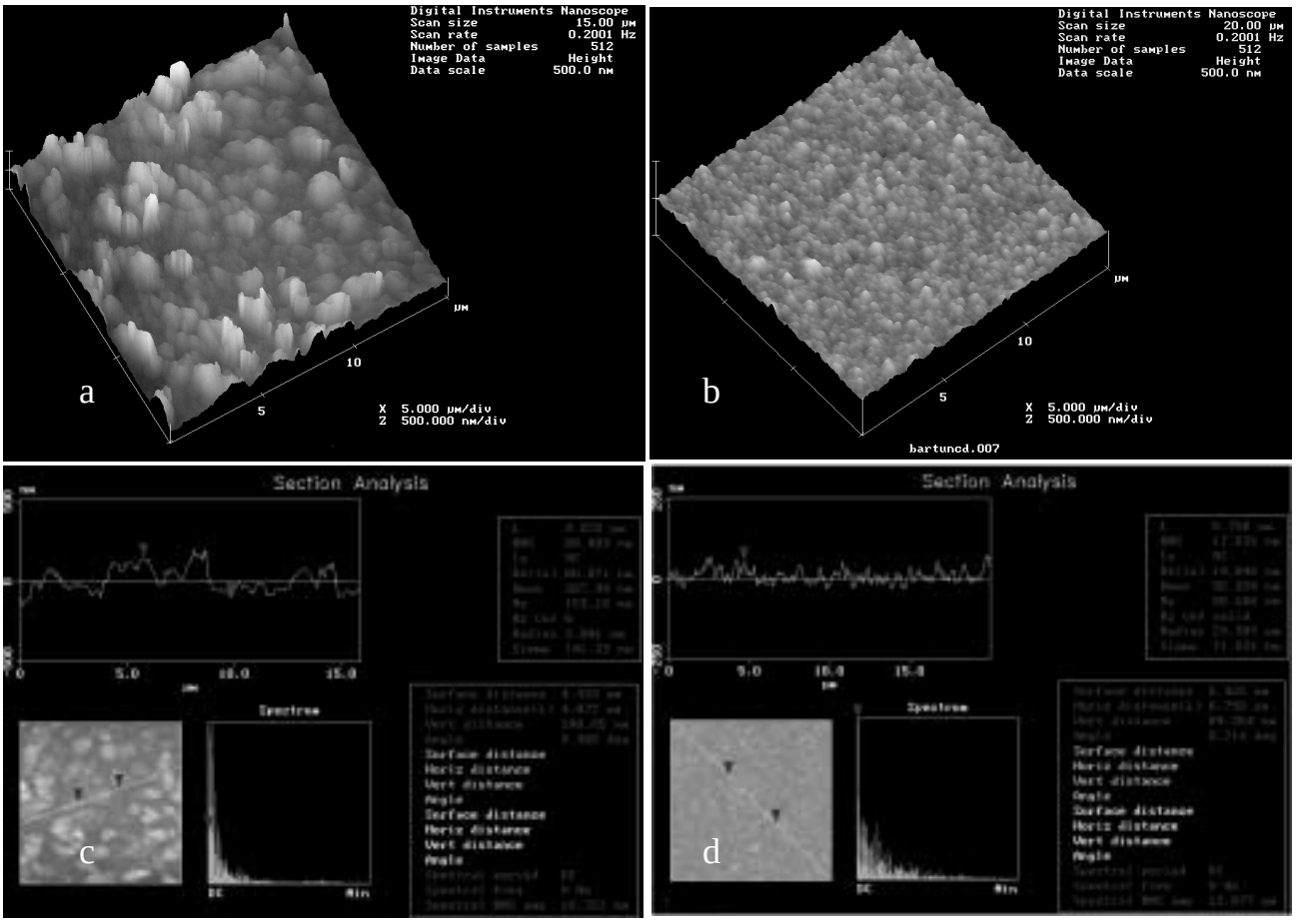

Fig. 11—3D surface profiles of UNCD film obtained by AFM: (a) microseeding and (b) nanoseeding. Roughness analyses of the thin films: (c) rms = 80 nm and R_{max} = 268 nm for microseeding; (d) rms = 18 nm and Rmax = 85 nm for nanoseeding.

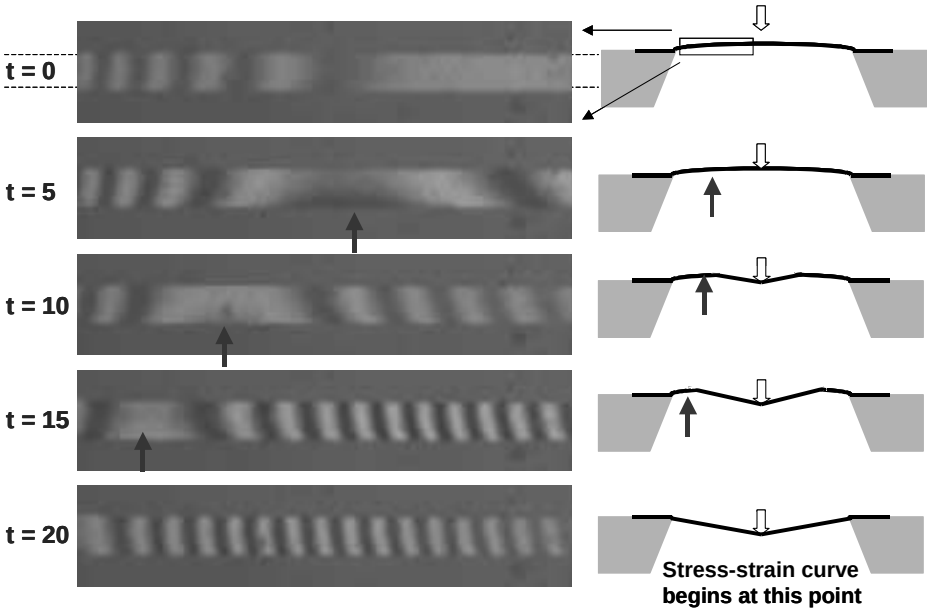

Fig. 12—Optical interferometric images of the MDE specimen gaged region at five different time intervals with corresponding side-view schematic diagram showing the *x-z* profile of the membrane. The solid arrow denotes the position of the curvature inflection point and the outlined arrow the position of the nanoindenter tip. Uniform straining begins at the last frame and represents the beginning of the computed stress-strain response.

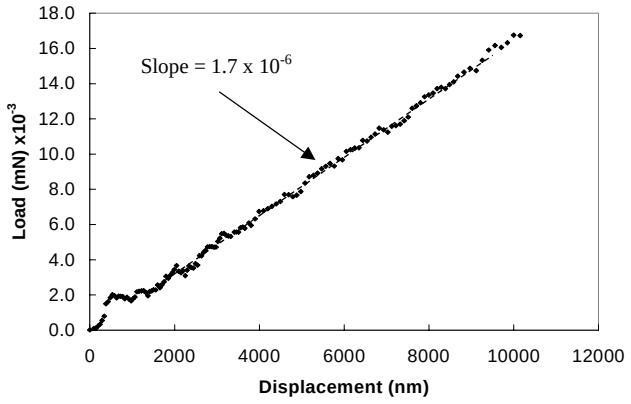

Fig. 13—Load-deflection curve for an 80 μm long cantilever. The slope, obtained from minimum square fit, represents the cantilever stiffness.

remains at this level for a period of time before increasing with deflection in a linear manner. The extrapolation of this linear region back to the zero-load and zero-displacement origin indicates that this phenomenon is likely due to various mechanisms occurring when contact is being made between the two bodies.

The slope of the linear region in Fig. 13 represents the elastic stiffness, k, of the UNCD cantilever. Using the parameters l = 80 μm, l_u = 15.32 μm, k = 1.7 N m^{-1}, t = 0.6305 μm, and b = 20 μm for the cantilever; eq (2) provides the equivalent length, l_{eq} = 88.2 μm, and eq (1) the Young's modulus, E = 937 GPa. This value is higher than the modulus measured by nanoindentation, which yielded an average value of 886 GPa.[9] Results of stiffness for several other cantilevers are given in Table 2. Measured values of elastic modulus for thin-film UNCD ranged from 916–959 GPa, subset (a) in Table 2. This scatter is the result of experimental errors associated to small inaccuracies in measuring film thickness.

Deflection tests for different cantilever lengths were also performed successively on the same cantilever by applying the contact force at lengths of 60, 80, 100, and 120 μm. The load–displacement responses are compared in Fig. 14. Each length exhibited linear behavior after contact with the cantilever surface. The stiffness increased proportionally as the cantilever length decreased in accordance with eq (1). The elastic modulus was calculated for each length and is listed in Table 2 as subset (b). Values of 937, 938, 957 and 958 GPa were obtained for cantilever lengths of 60–120 μm, respectively. All values fall well within the range measured in subset (a) where all cantilevers had a length of 80 μm. Although these results suggest a transition from lower to higher modulus between lengths of 60–80 μm and 100–120 μm, we believe this is not a real trend but only a manifestation of the normal scatter and experimental error of the technique. Since the tests were performed on the same cantilever where each test uses the same measured thickness, this error represents irregularities in measured stiffness and/or in the positioning of the nanoindenter tip with respect to the beam fixed support.

Deflection tests were also performed successively on the same cantilever to examine repeatability of the technique. Figure 15 shows the load–displacement curves for four successive tests on the same cantilever. The curves and measured stiffness match well between tests. Values of stiffness and calculated elastic modulus are listed as subset (c) in Table 2. Stiffness varied from 1.49 to 1.52 N m^{-1} with corresponding varying moduli of 931–956 GPa. These data provide confidence in the repeatability of the cantilever-based experiments to yield measured stiffness and modulus values to within 2.7 percent error. As with the different cantilever length tests

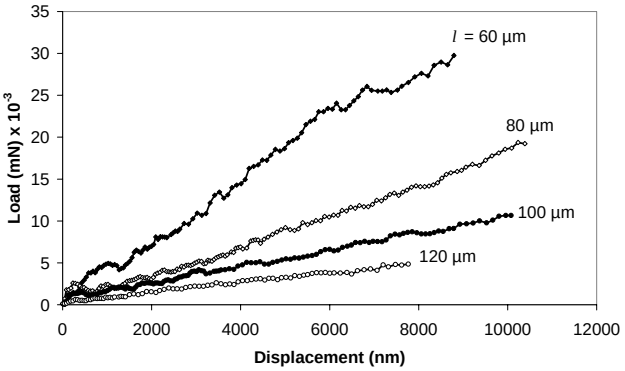

Fig. 14—Load-displacement curves for a concentrated load applied at lengths of 60, 80, 100, and 120 µm. All tests are performed on the same cantilever.

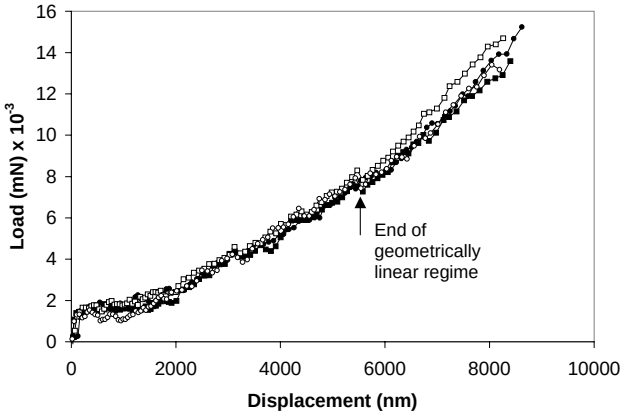

Fig. 15—Load-displacement curves for four different deflection experiments on the same cantilever and at a constant length of 80 µm where the concentrated load is applied. The variability in the data increases at the end of the geometrically linear regime, which corresponds to a deflection of about 5.7 µm.

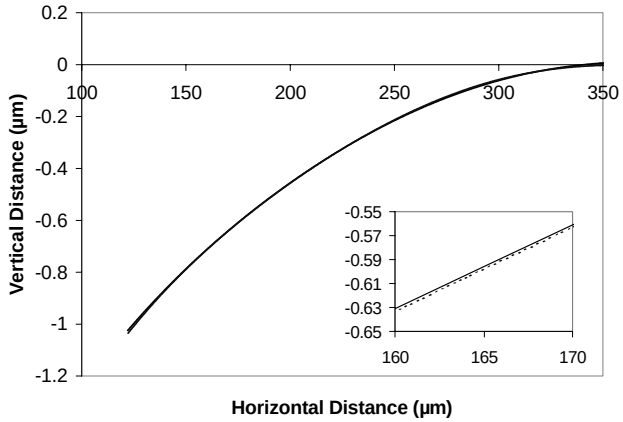

Fig. 16—Comparison of cantilever z-profiles before and after deflection testing. The plot inset is a zoom to discern the two curves. The observed differences in deflection are a fraction of a nanometer.

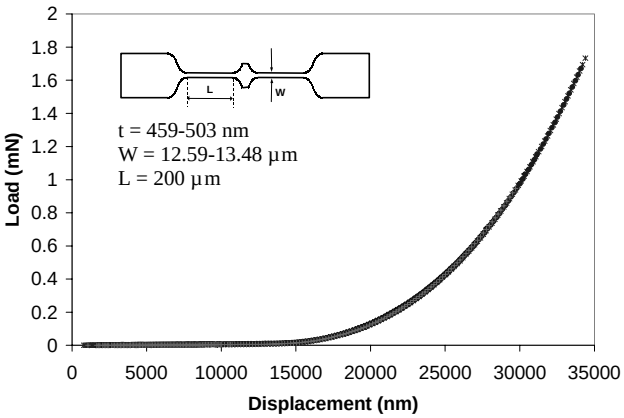

Fig. 17—Load-displacement signatures of four different UNCD MDE tests

reported above, it should be noted that this error stands only for the sensitivity aspects of the stiffness measurement and length measurement and not for errors involved in accurately measuring film thickness.

The cantilevers were examined for signs of plasticity by characterizing the specimen z-profile before and after loading using a MicroXAM 3-D full-field surface profilometer with nanometer resolution. Figure 16 is a plot comparing profiles before and after a deflection test. These curves represent the vertical cross-section along the cantilever length. The curves are almost identical and only the extreme zoom in the plot inset can discern their differences. Since the deviation is only of the order of a few nanometers, we can conclude that the cantilever deformation did not exceed the elastic limits of the UNCD films.

Membrane Deflection Experiments

Figure 17 shows the load–displacement signatures for several of the membrane deflection experiments. The response of the individual membranes is uniform from sample to sample with each exhibiting a statistical variation in failure point. The stress–strain behavior was obtained using equations (3)–(6) and it is shown in Fig. 18. The data shown in the figure begin at a deflection where the membrane becomes stretched in pure tension, state 3 in Fig. 3. The stress–strain response increases in a linear fashion until failure at 5.03 GPa. The slope of the plot represents the elastic modulus and was found to be 959 GPa. Measured values for elastic modulus of microseeded samples ranged between 930–970 GPa and between 945–963 GPa for the nanoseeded samples.

A final aspect that can be highlighted from the plot reported in Fig. 18 is the extrapolation of the linear elastic region to zero strain. This point represents a good estimate of the applied stress, of about 100 MPa, needed to transition from state 1 to state 3 as described in the characterization section.

The plot in Fig. 18 represents the highest fracture strength measured by the MDE technique. Fracture strength varied in a statistical manner. In all specimens tested, failure occurred in the gauged region. This is illustrated in Fig. 19, which shows two UNCD membranes tested to failure. The

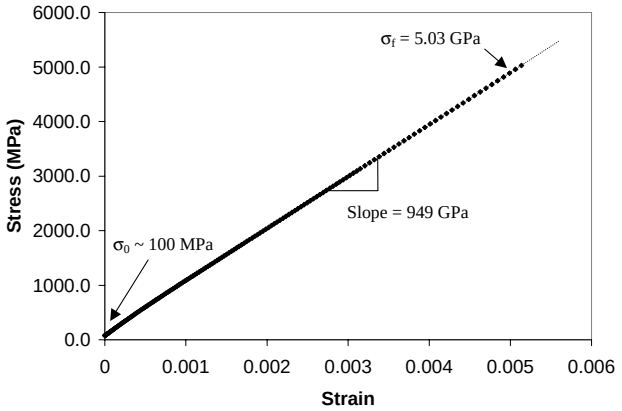

Fig. 18—Stress-strain curve representative of a typical UNCD MDE sample. An elastic modulus of 949 GPa, a fracture stress of 5.03 GPa, and an estimated initial stress of 100 MPa were identified.

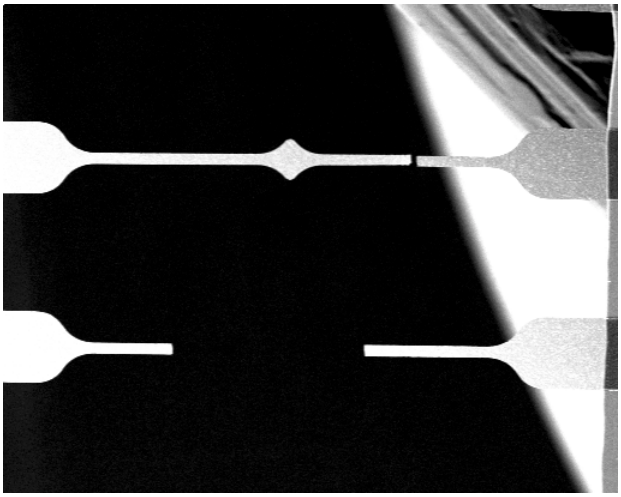

Fig. 19—SEM image of two MDE specimens after testing. Both membranes show that failure occurs in the gaged regions where axial deformation is uniform.

upper sample has failed on the right-hand gage while the bottom sample has failed simultaneously in both gaged regions. Fracture strength varied from 0.89 to 2.42 GPa for the microseeded samples and from 3.95 to 5.03 GPa for the nanoseeded samples. The variation is believed to result from differences in specimen flaws generated during the seeding, deposition, and microfabrication processes. We attribute the low fracture values of the microseeded samples to scratch-like and other defects identified on the film surface as shown in the inset of Fig. 3. We believe that these defects originated from the seeding process used to grow the UNCD films and that they affect the fracture strength more than the material moduli. The new nanoseeding process significantly reduced the surface roughness and eliminated scratch-like and other surface defects. As a result, the process not only reduced the spreading in measured elastic modulus but also more than doubled the film fracture strength. It is expected that further improvements in processing can improve fracture strength to even higher values.

Table 3 summarizes the results on both microseeded and nanoseeded specimens tested by the MDE technique. The measured properties are very promising when compared to other common MEMS materials; see Table 4. The elastic modulus is considerably higher than that for single-crystal Si, polycrystalline Si, SiC, Si_3N_4, or diamond-like carbon (literature references for these materials are given in Table 4). The fracture strength of UNCD is also unmatched. The results of this work demonstrate the significant mechanical advantages that UNCD can provide to MEMS/NEMS devices. When combined with the other significant properties mentioned in the introduction, it is clear that UNCD is poised to gain attention in the field.

Conclusions

In this work, microcantilever deflection and membrane deflection experiments were used to determine the elastic modulus and strength of UNCD thin films. Values of modulus ranging from 916 to 959 GPa were measured with the cantilever deflection technique. A comparison of cantilever topography before and after deflection testing reveals identical shape and suggests that the elastic limit of UNCD was not exceeded. The largest source of error in the method was believed to be inaccurate measurement of the film thickness, which in the modulus calculation is cubed and in the denominator, see eq (1). The test was also verified by deflecting a single-crystal silicon cantilever of a common AFM tapping-mode tip. The elastic modulus measured was consistent with the literature value of 170 GPa in the [110] direction.

Characterization of the UNCD films by the MDE yielded elastic modulus values between 930–970 GPa for the microseeded samples and between 945–963 GPa for the nanoseeded samples. These results agreed well with those obtained by the microcantilever-based technique and prior measurements using nanoindentation,[9] although the MDE results exhibited a smaller degree of variability. The fracture strength of the UNCD membrane varied from 0.89 to 2.42 GPa for the microseeded samples and from 3.95 to 5.03 GPa for the nanoseeded samples. This increase is believed to result from fewer flaws through the nanoseeding process. The out-of-plane initial shape of the MDE membranes challenged the data reduction; however, its careful consideration in the data processing allowed for an interpretation of the material response in pure tension. Future work will involve a more in-depth study of fracture behavior with specimens of a more uniform size and with fewer and smaller flaws through better control of the wafer processing variables.

The characterization of mechanical properties of thin-film-based MEMS structures, such as those discussed in this paper, is quite challenging because properties may depend not only on the intrinsic microstructure or composition of the material but also on specific features of the film manufacturing process. In this work, reliable data on material properties were extracted by the utilization of microscale testing methodologies. The results of both testing methods used in the work discussed here yielded very similar elastic modulus values, although the cantilever deflection technique was only able to characterize the material's elastic modulus and not the strength. The MDE method proved to be more versatile and yielded other material properties such as fracture

TABLE 3—VALUES OF ELASTIC MODULUS AND FRACTURE STRENGTH FROM MEMBRANE DEFLECTION TESTS

Sample	Elastic Modulus (GPa)	Fracture Strength (GPa)
Microseeding		
1	934	0.89
2	970	1.12
3	942	1.17
4	928	1.26
5	933	1.37
6	966	1.41
7	964	1.59
8	940	1.60
9	944	1.65
10	941	1.70
11	957	1.71
12	948	2.42
Nanoseeding		
1	960	3.95
2	963	4.00
3	945	4.21
4	958	4.33
5	949	5.03

TABLE 4—VALUES OF ELASTIC MODULUS AND FRACTURE STRENGTH OF TYPICAL MEMS MATERIALS

Materials	Elastic Modulus (GPa)	Fracture Strength (GPa)	
UNCD (this work)	941–963	3.95–5.03	This work
UNCD	967	–	Sumant et al.[9]
Si (single crystal)	150	0.3	Peterson[28]
Poly-Si	158 ± 8	1.56 ± 0.25	Sharpe et al.[29]
	157 ± 6	3.09 ± 0.18	Jackson et al.[30]
SiC	373	1.44	Lohner et al.[31]
	440	0.51	Henshall et al.[32]
Si_3N_4	254 ± 3	1.6	Coles et al.[33]
Diamond-like Carbon (DLC)	800	0.7	Christiansen et al.[34]

strength. Likewise, the relevance of surface finishing on specimen properties was assessed. The inference is that the MDE method is more suited for obtaining mechanical property data on micrometer and submicrometer films since it can subject the free-standing films to direct tension while independently and directly measuring load and deflection. It also has the added advantage of yielding both residual and yield/fracture stress of the material.[25]

Acknowledgments

This work was sponsored by the National Science Foundation under Career Award No CMS-9624364 and under GOALI Award No CMS-0120866/001. This work was also supported in part by the Nanoscale Science and Engineering Initiative of the National Science Foundation under NSF Award Number EEC-0118025 and by DOE Office of Science under contract No N00014-97-1-0550.

References

1. Bustillo, J.M., Howe, R.T., and Muller, R.S., "Surface Micromachining for Microelectromechanical Systems," Proc. IEEE, **86**, *1552–1574 (1998).*

2. Sniegowski, J.J. and de Boer, M.P., "IC-compatible Polysilicon Surface Micromachining," Annu. Rev. Mater. Res., **30**, *299–333 (2000).*

3. Bhushan, B., Tribology Issues and Opportunities in MEMS, Kluwer Academic, Dordrecht (1998).

4. de Boer, M.P. and Mayer, T.M., "Tribology of MEMS," MRS Bulletin, **4**, *302–304 (2001).*

5. Gruen, D., "Nanocrystalline Diamond Films," Annu. Rev. Mater. Sci., **29**, *211–259 (1999).*

6. Gruen, D.M., Liu, S., Krauss, A.R., Luo, J., and Pan, X., "Fullerenes as Precursors for Diamond Film Growth without Hydrogen or Oxygen Additions," Appl. Phys. Lett., **64**, *1502–1504 (1994).*

7. Gruen, D.M., Liu, S., Krauss, A.R. and Pan, X., "Buckyball Microwave Plasmas: Fragmentation and Diamond-film Growth," J. Appl. Phys., **75**, *1758–1763 (1994).*

8. Bhattacharyya, B., Auciello, O, Birrell, J., Carlisle, J.A., Curtiss, L.A., Goyette, A.N., Gruen, D.M., Krauss, A.R., Schlueter, J., Suman, A., and Zapol, P., "Synthesis and Characterization of Highly-conducting Nitrogen-Doped Ultrananocrystalline Diamond Films," Appl. Phys. Lett., **79**, *1441–1443 (2001).*

9. Sumant, A.V., Auciello, O., Krauss, A.R., Gruen, D.M., Ersoy, D., Tucek, J., Jayatissa, A., Stach, E., Moldovan, N., Mancini, D., Busmann, H.G., and Meyer, E.M., "Fabrication of MEMS Components Based on Ultrananocrystalline Diamond Thin Films and Characterization of Mechanical Properties," Mater. Res. Soc. Symp. Proc., **657** *(2000).*

10. Erdemir, A., Fenske, G.R., Krauss, A.R., Gruen, D.M., McCauley, T., and Csencsits, R.T., "Triboligical Properties of Nanocrystalline Diamond Films," Surf. Coat. Technol., **120–121**, *565–572 (1999).*

11. Krauss, A.R., Auciello, O., Ding, M.Q., Gruen, D.M., Huang, Y., Zhirnov, V.V., Givargizov, E.I., Breskin, A., Chechen, R., Shefer, E., Konov, V., Pimenov, S., Karabutov, A., Rakhimov, A., and Suetin, N., "Electron

Field Emission for Ultrananocrystalline Diamond Films," J. Appl. Phys., **89**, *2958–2967 (2001).*

12. Zapol, P., Sternberg, M., Curtiss, J., Frauenheim, T., and Druen, D.M., "Tight-binding Molecular-dynamics Simulation of Impurities in Ultrananocrystalline Diamond Grain Boundaries," Phys. Rev. B, **65** *(2002).*

13. Gruen, D.M., Krauss, A.R., Zhou, D., McCauley, T.G., and Corrigan, T.D., in Chemical Vapor Deposition, M.D. Allendorf and C. Bernard, eds, 97–25, 325–32, Electrochem. Soc, Pennington Publishers, NJ (1997).

14. Auciello, O., Krauss, A.R., Gruen, D.M., Busmann, H.G., Meyer, E.M., Tucek, J., Sumant, A., Jayatissa, A., Moldovan, N., Mancini, D.C., and Gardos, M.N., "Two- and Three-dimensional Ultrananocrystalline Diamond (UNCD) Structures for a High Resolution Diamond-based MEMS Technology", Mater. Res. Soc. Symp. Proc., **605**, *73–78 (2000).*

15. Moldovan, N., Auciello, O., Sumant, A.V., Carlisle, J.A., Divan, R., Gruen, D.M., Krauss, A.R., Mancini, D.C., Jayatissa, A., and Tucek, J., "Ultrananocrystalline Diamond Thin Films for MEMS and Moving Mechanical Assembly Devices," International Symposium on Micromachining and Microfabrication, 22–25 October 2001, San Francisco, CA, Proc. SPIE, **4557**, *288–298 (2001).*

16. Nix, W.D., "Mechanical Properties of Thin Films," Metall. Trans. A, **20**, *2217–2245 (1989).*

17. Brotzen, F.R., "Mechanical Testing of Thin Films," Int. Mater. Rev., **39**, *24–45 (1994).*

18. Kraft, O. and Volkert, C., "Mechanical Testing of Thin Films and Small Structures," Adv. Eng. Mater., **3**, *99–110 (2001).*

19. Weihs, T.P., Hong, S., Bravman, J.C., and Nix, W.D., "Mechanical Deflection of Cantilever Microbeams: A New Technique for Testing the Mechanical Properties of Thin Films," J. Mater. Res., **3**, *931–942 (1988).*

20. Schweitz, J.-A., "Mechanical Characterization of Thin Films by Micromechanical Techniques," MRS Bull., **17**, *34–45 (1992).*

21. Kraft, O., Schwaiger, R., and Nix, W.D., "Measurement of Mechanical Properties in Small Dimensions by Microbeam Deflection," Mater. Res. Soc. Symp. Proc., **518**, *39–44 (1998).*

22. Espinosa, H.D., Fischer, M., Zhu, Y., and Lee, S., "3-D Computational Modeling of RF MEMS Switches," Proceedings of the 4th International Conference on Modeling and Simulation of Microsystems, M. Laudon and B. Romanowicz, eds, 402–405 (2001).

23. Espinosa, H.D., Prorok, B.C., Zhu, Y., and Fischer, M., "An Investigation of Plasticity in MEMS Materials," Proceedings of InterPACK '01, 8–13 July, Kauai, Hawaii, USA (2001).

24. Espinosa, H.D., Prorok, B.C., and Fischer, M., "A Novel Experimental Technique for Testing Thin Films and MEMS Materials," Proceedings of the SEM Annual Conference on Experimental and Applied Mechanics, 4–6 June, Portland, Oregon, 446–449 (2001).

25. Espinosa, H.D., Prorok, B.C., and Fischer, M., "A Methodology for Determining Mechanical Properties of Free-standing Thin Films and MEMS Materials," Journal of the Mechanics and Physics of Solids, **51**, *47–67 (2003).*

26. Fischer, M., "MEMS Materials Testing," Master Thesis, Purdue University, West Lafayette, IN (1999).

27. Burenkov, Y.A. and Nikanorov, S.P., "Temperature Dependence of the Elastic Constants of Silicon," Sov. Phys.-Solid State, **16**, *963–964 (1974).*

28. Peterson, K.E., "Silicon as a Mechanical Material," Proc. IEEE, **70** *(5) (1982).*

29. Sharpe, W.N., Jr., Jackson, K., Coles, G., and LaVan, D.A., "Mechanical Properties of Different Polysilicons," ASME Symposium on Micro-Electro-Mechanical Systems (MEMS), Orlando, FL, Vol. 2 (2000).

30. Jackson, K.M., Bucheit, T.E., and LaVan, D.A., "Fracture Toughness of Thin Film Polysilicon Used in MEMS Devices," Proceedings of the MEMS, Society of Experimental Mechanics, 11–15 (2001).

31. Lohner, K.A., Chen, K.-S., Ayon, A.A., and Spearing, S.M., "Microfabricated Silicon Carbide Microengine Structures," Mater. Res. Soc. Symp. Proc., **546**, *85–90 (1999).*

32. Henshall, J.L., Rowcliffe, D.J., and Edington, J.W., "Fracture Toughness of Single Crystal Silicon Carbide," J. Am. Ceram. Soc., **60** *(1977).*

33. Coles, G., Sharpe, W.N., Jr., and Edwards, R.L., "Mechanical Properties of Silicon Nitride," Proceedings of MEMS: Mechanics and Measurement Symposium, Society of Experimental Mechanics, 1–4 (2001).

34. Christiansen, S., Albrecht, M., and Strunk, H.P., "Mechanical Properties and Microstructural Analysis of a Diamond-like Carbon Coating on an Alumina/glass Composite," J. Mater. Res., **11** *(8) (1996).*

35. Auciello, O., Gruen, D.M., Krauss, A.R., Jayatissa, A., Sumant, A., Tucek, J., Mancini, D.C., Moldovan, N., Erdemir A., Ersoy, D., Gardos, M.N., Busmann, H.G., and Meyer, E.M., SPIE 2000 Symposium on "Smart Materials and MEMS," Melbourne, Australia, 13–15 December, Proc. SPIE (2001).

36. Bobji, M.S. and Biswas, S.K., "Deconvolution of Hardness from Data Obtained from Nanoindentation of Rough Surfaces," J. Mater. Res., **14**, *2259–2268 (1999).*

37. Krauss, A.R., Auciello, O., Gruen, D.M., Jayatissa, A., Sumant, A., Tucek, J., Mancini, D.C., Moldovan, N., Erdemir, A., Ersoy, D., Gardos, M.N., Busmann, H.G., Meyer, E.M., and Ding, M.Q., "Ultrananocrystalline Diamond Thin Films for MEMS and Moving Mechanical Assembly Devices," Diam. Relat. Mater., **10**, *1952–1961 (2001).*

